TID- Brown

8977-6028-SU-000

TID-17005

# KINETIC STUDIES OF HETEROGENEOUS WATER REACTORS



## September 1962 Quarterly Progress Report

prepared for

U. S. ATOMIC ENERGY COMMISSION
SAN FRANCISCO OPERATIONS OFFICE
Berkley, California

CONTRACT NO. AT(04-3)-372

30 SEPTEMBER 1962



SPACE TECHNOLOGY LABORATORIES, INC.
A SUBSIDIARY OF THOMPSON RAMO WOOLDRIDGE, INC.
ONE SPACE PARK • REDONDO BEACH, CALIFORNIA

## DISCLAIMER

8977-6028-SU-000

11 October 1962

# Quarterly Progress Report

## for Period Ending 30 September 1962

## Report No. 21



"KINETIC STUDIES OF

HETEROGENEOUS WATER REACTORS"

Prepared for:

U. S. Atomic Energy Commission
Berkeley, California

Contract No. AT(04-3)-372

Prepared by:

W. W. Brown
L. Wentz
R. W. Wright
G. C. K. Yeh
S. M. Zivi, Project Manager

Approved by

D. B. Langmuir
Director

PHYSICAL ELECTRONICS LABORATORY
Physical Research Division

SPACE TECHNOLOGY LABORATORIES, INC.
8433 Fallbrook Avenue
Canoga Park, California

## ACKNOWLEDGEMENT

The assistance of Professors S. G. Bankoff and L. O. Roellig as scientific consultants during this quarter is acknowledged with thanks.

Messrs. G. H. Humberstone, R. A. Briones, R. L. Mason and R. J. Siewert contributed greatly to the design and construction of the experimental apparatus described herein.

TABLE OF CONTENTS

# KINETIC STUDIES OF HETEROGENEOUS WATER REACTORS

## I. INTRODUCTION

During the quarter ending on September 30, 1962, two experiments were designed and built, in preparation for the measurement of transient steam void formation and extreme pressure pulses during severe power excursions under reactor-like conditions. The first of these experiments is an in-pile capsule experiment to be carried out using the KEWB reactor as a pulsed source of neutrons. The water-filled capsule, which will be exposed to the neutron flux in the reactor's experimental facility, will contain a uranium bearing plate. The transient heating of the plate will produce a surface temperature transient which is characteristic of a severe power excursion in a heterogeneous water reactor. The measurements of steam formation rates in this experiment will be applicable to the destructive transients presently underway in the SPERT I reactor. It is anticipated that the reactor period in this series of SPERT tests may be as short as 2 milliseconds, and therefore exponential periods between 5 and 1 millisecond are of primary interest in our capsule experiment. The preparations for this experiment are described in Part II.

The second experiment developed during this quarter is an out-of-pile apparatus wherein an attempt will be made to create severe pressure transients (about 8000 psi) by causing the temperature of a surface to rise rapidly through the thermodynamic critical point of water. It was postulated in our March 1962 quarterly report[1], that the extreme pressure transients observed in the BORAX I experiment might be attributed to rapid heating of the thin film of water in immediate contact with the fuel surfaces of the reactor. The postulated mechanism

requires a large surface area per unit volume of core, as well as the very rapid heating of that surface. Each of these two requirements creates difficult design problems for an out-of-pile experiment, as discussed in Part III. It is expected that the first experiments will be carried out during the next quarter.

Studies related to boiling water reactor stability continued during this quarter. The experimental work consisted of a continuation of the transfer function and steam void fraction distribution measurements presented in our earlier reports, and the analytical effort was directed at the prediction of multi-channel behavior from measurements on a single natural circulation boiling channel. The results of this analysis are presented in Part IV of this report, where it is shown that a multi-channel natural circulation boiling system may have two modes of hydrodynamic instability. The first mode is identical to the single-channel hydrodynamic instability which may be observed in the laboratory. In this mode, the flow oscillations in the numerous channels are in phase with each other. In the other possible mode of oscillations (assuming identical channels) the gross flow rate into the ensemble of channels remains constant, because the phase relationships of individual channel flow oscillations result in complete cancellation of the disturbance when the separate flows are combined. The latter mode of instability is identical to the case of instabilities under forced circulation in parallel channels. This analysis is continuing.

## II. PREPARATIONS FOR THE MEASUREMENT OF TRANSIENT STEAM VOID FORMATION IN VERY RAPID POWER EXCURSIONS* (W. W. Brown and L. B. Wentz)

### A. The Experimental Apparatus

The experiments described in the following are to be performed with the KEWB reactor which is capable of repeatedly generating exponential power transients down to 1 millisecond period. The transients are of sufficient power to raise the temperature of small fuel samples a few hundred degrees if they are placed near the core. A capsule has been constructed to contain such a fuel sample, in the form of a disc, surrounded by water. It is designed so that it can be placed near the reactor core and, at the same time, permit photographic observation of the fuel disc and recording of surface temperature, internal pressure, and void production. These observations will be made over a range of reactor periods extending from about 1 to 15 milliseconds. Other parameters that will be varied include initial temperature, initial pressure, inertial loading, and the enrichment of the uranium in the fuel disc. This report describes the capsule and its operation. Also described is an approximate calculation of the temperature distribution in the fuel and water during a transient. This is for use as a guide during the performance of the experiment. For later analysis a more accurate means of calculation, employing a digital computer, has been prepared.

The capsule consists essentially of three main parts; a front chamber containing the fuel disc and the water surrounding it; a piston and shaft to communicate void formed in the front

---

*The advice and cooperation of Mssrs. M. Silberberg, R. Cordy, and C. Bumpus of Atomics International and Mr. R. Miller of Phillips Petroleum Co. is gratefully acknowledged.

chamber to a linear motion transducer; and a rear chamber surrounding the transducer and piston shaft. The static pressure in the front chamber can be adjusted to any desired value by control of the gas pressure in the rear chamber.

A cross section of the capsule is shown in Figure 1. The fuel disc, 1.25 inches in diameter and 20 mils thick, consists of an alloy of uranium and molybdenum (10% Mo by weight). It is clad with aluminum 5 mils thick around the edge and 3 to 4 mils thick on the flat surfaces. The volume of water surrounding the fuel is purposely kept small (to about 5 $cm^3$) so that extraneous void production by either gamma ray heating or radiolysis is minimized. The 5 $cm^3$ includes the water up to the shut-off valves on the inlet and outlet water lines. The sapphire window permits photographic observation of one side of the disc during a transient. Sapphire is sufficiently radiation resistant to ensure that its transmission will remain good for many transients. The window and body of the capsule have been designed to withstand pressures up to 10,000 psi. In later phases of the experiment, transient pressures of this magnitude may occur and the capability for measuring them will be needed. The piston shaft carries an inertial load which can be varied from about 200 to 800 grams so that conditions equivalent to the water head existing above the core in a reactor can be created. The probe attached to the end of the shaft is the moving element of the linear motion transducer. The time record of this motion provides a direct measure of any void volume change occurring in the chamber containing the fuel and water. A pressure transducer communicates with the front chamber through the water inlet line. Six thermocouples are attached at various points to the surface of the disc. Time records of the signals from the pressure and temperature detectors will also be made. The initial pressure, if it is required to be different from

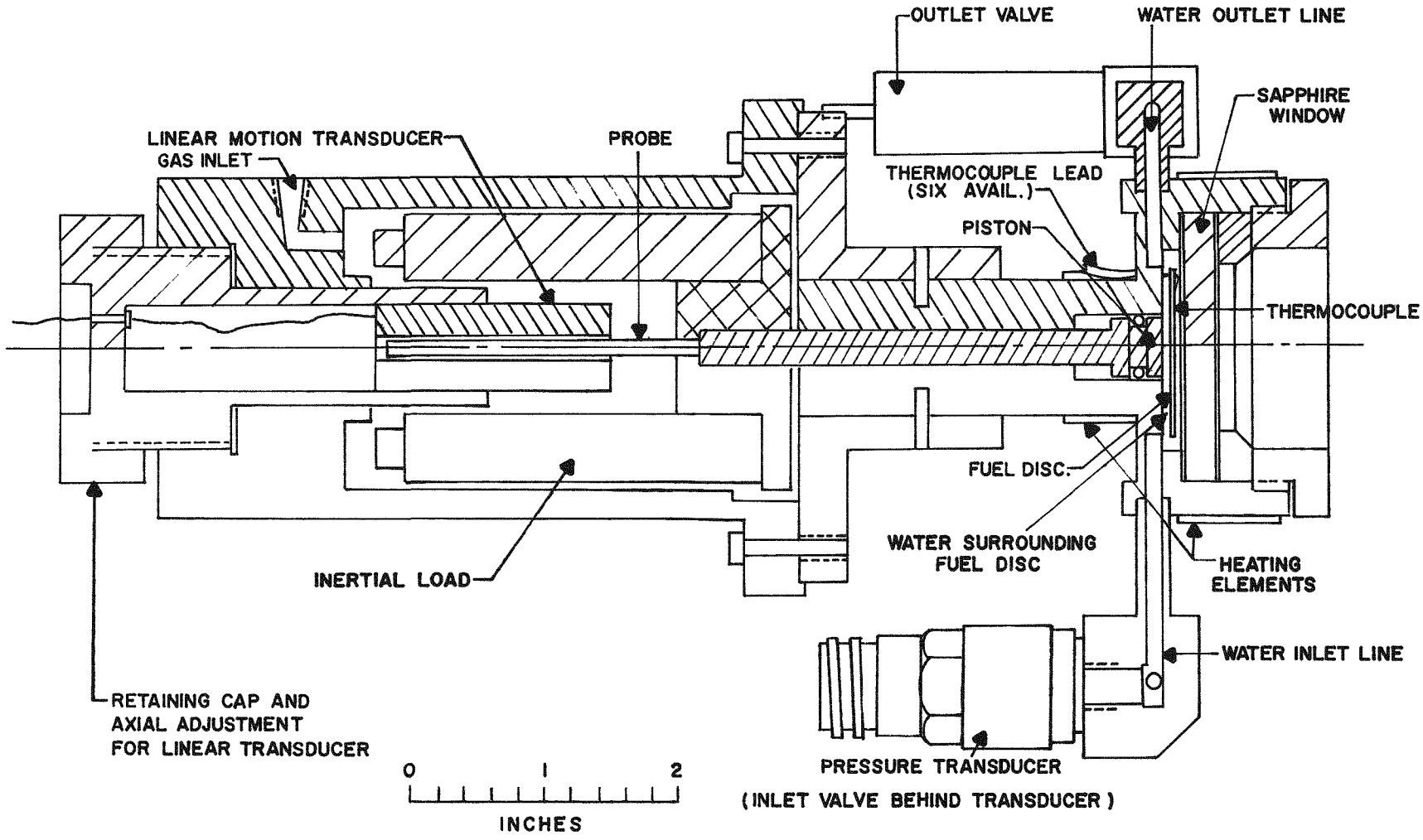


Figure 1. Capsule Design for In-Pile Experiments on Steam Formation in Severe Power Excursions.

atmospheric, can be set remotely through a gas line connected to the rear chamber. Initial temperatures up to 150°C can be set by means of the heaters attached to the outer surface of the capsule near the front chamber.

Because of the need to fill the capsule with new water following each transient, a water handling apparatus has been constructed which can be located near the reactor. The arrangement is shown schematically in Figure 2. Commercially distilled water from the reservoir is pumped into the degassing chamber through a demineralizer and submicron filter. The water is there agitated with a paddle wheel while under vacuum to remove dissolved gas and then admitted to the front chamber of the capsule. The extent to which trapped gas remains in the chamber can be estimated by taking the following steps: Pressurizing the rear chamber, measuring the amount that the piston moves, and comparing this with what would be expected from the combined compression of water and mechanical compliance of the capsule. Following each transient, the compliance measurement will be repeated to detect radiolytic gas, and then the water in the capsule will be drained into a reservoir. Samples can be taken from the reservoir to test for the presence of radioactivity and to repeat the gas content measurement. The radioactivity test will indicate whether or not a cladding rupture has occurred, and the measurement of gas content (dissolved) will detect any extensive radiolysis of the water.

The location of the capsule and water system in the KEWB reactor room is shown in Figure 3. The capsule is contained in a rectangular aluminum box which fits into the 8 inch x 8 inch exposure facility. The facility runs horizontally through the graphite reflector. At its nearest point beside the core the central axis of the facility is about 12 inches from the core

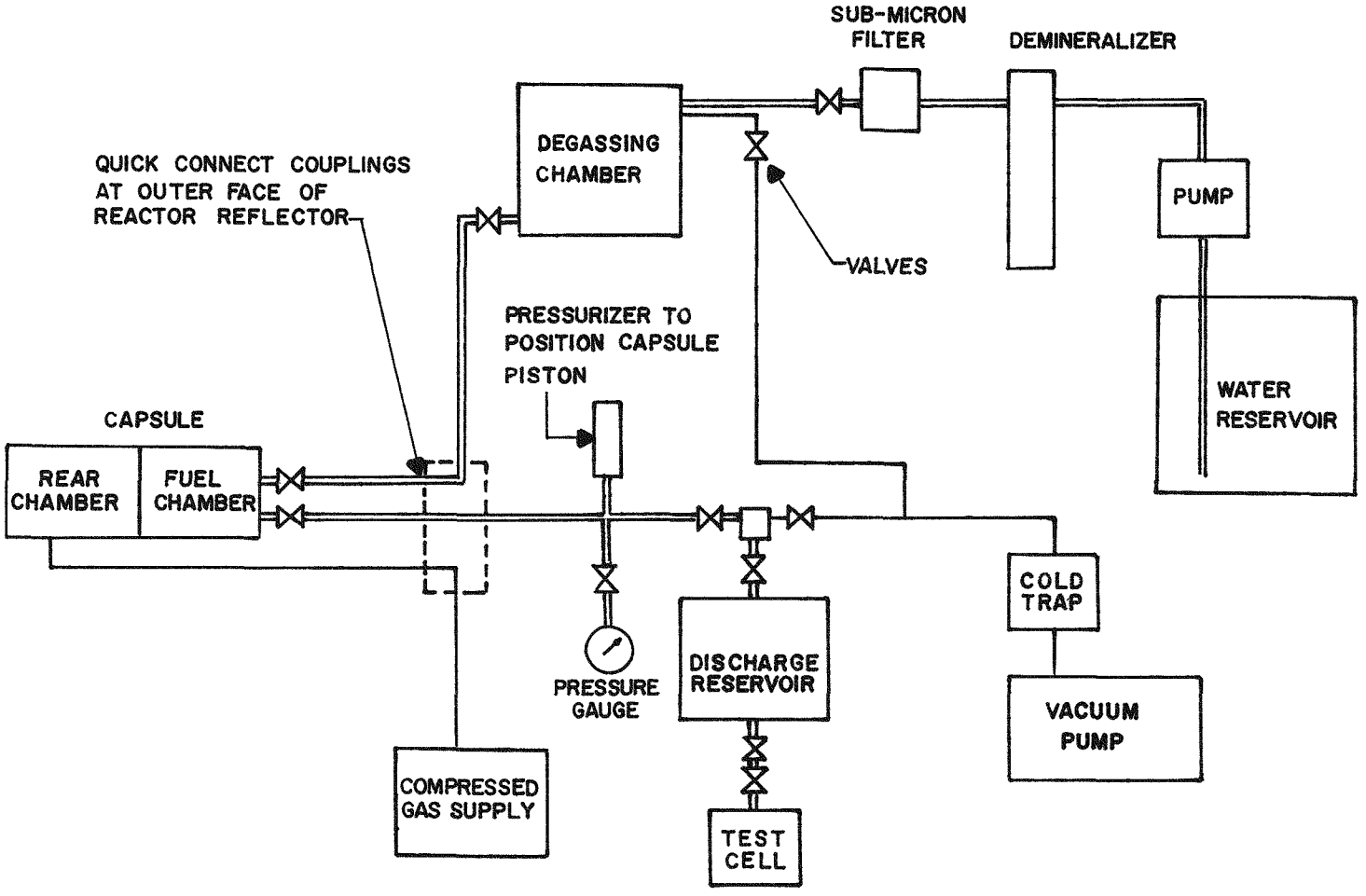


Figure 2. Schematic Diagram of the Apparatus for Degassing and Transferring the Capsule Water.

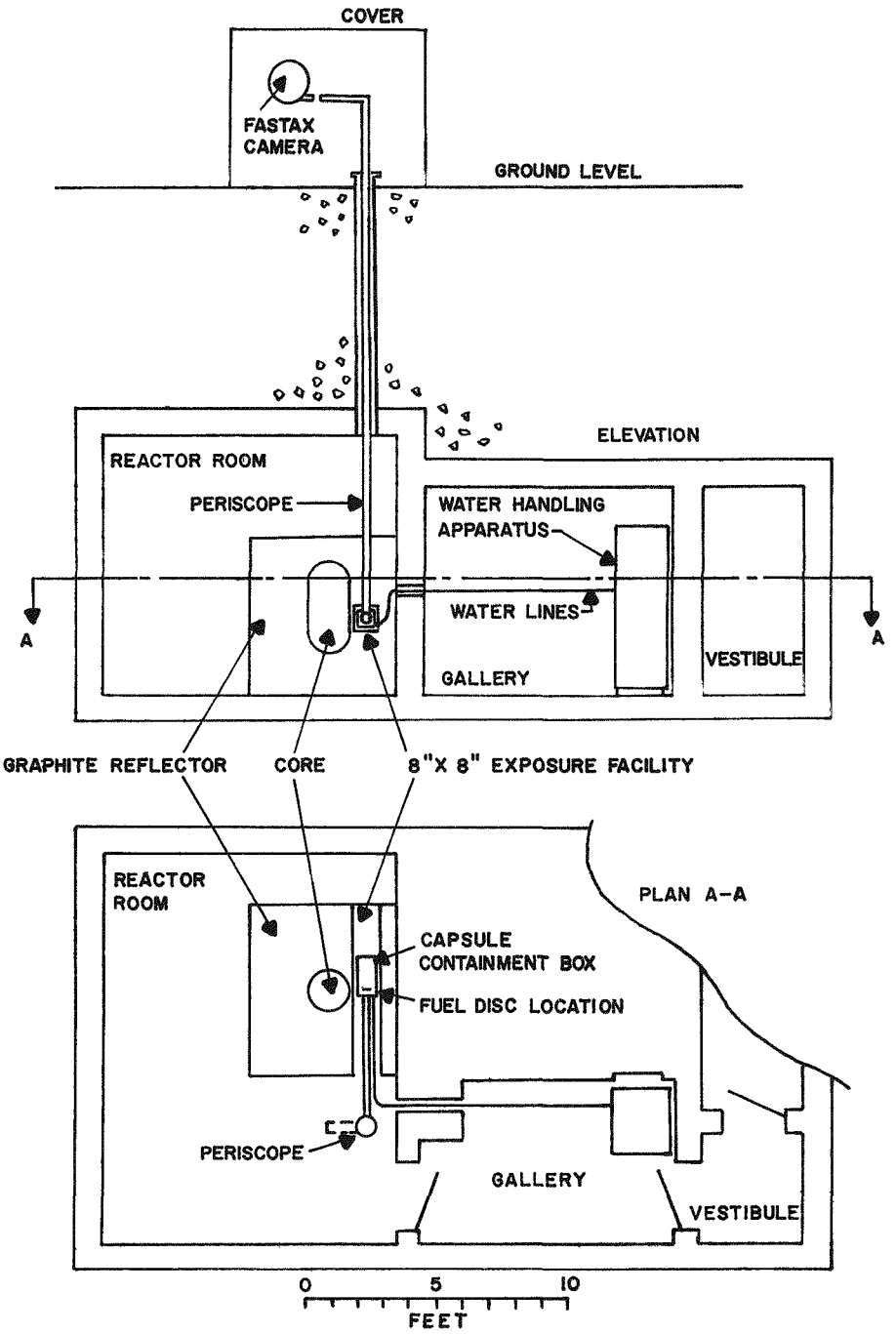


Figure 3. Overall Arrangement of the Capsule Experiment at the KEWB Site.

center. The capsule containment box is located so that the plane of the fuel disc is vertical and perpendicular to the core surface. Its center is then about 12 inches from the core center. Empty space within the box is filled, wherever possible, with graphite. A 1-1/2 inch diameter conduit carries the electrical and water lines from the capsule to the outside of the reactor reflector. A 3 inch diameter axial tube attached to the front end of the box and to the objective cell of the periscope provides a path for viewing the fuel disc through the sapphire window. The eye-piece of the periscope is located at ground level, exterior to the reactor room and about 20 feet above the capsule. A Fastax camera will be used with the periscope to obtain high-speed motion pictures of steam void formation during the power excursions. The space in the exposure facility not occupied by the containment box, periscope tube, and lead lines will be filled with graphite.

B. Estimates of Temperature Distributions

Before making the initial runs in the reactor, it is necessary to make an estimate of the fuel and water temperature histories likely to be met. The estimate would be used also during the course of the experiment to anticipate the changes in temperature history as we progress to transients of shorter and shorter periods. For this purpose an approximate calculation has been made. It is based on a one dimensional, three region solution of the heat equation

$$k \frac{\partial^2 T}{\partial x^2} + S = \rho c \frac{\partial T}{\partial t}$$

where T is the temperature, S is the heat source strength per unit volume, t the time, x the distance from the fuel center,

and k, $\rho$, and c are the thermal conductivity, density, and specific heat, respectively. It is assumed that the fuel, of half thickness a, and cladding of thickness (b-a), are infinite plates in an infinite body of water, and that the values of k, $\rho$, and c appropriate to each material remain constant at their room temperature values. If the heat source, S, is zero except in the fuel where it is uniform spatially but of time dependence $S = S_o e^{\alpha t}$, then the temperature at any time is

$$\left.\begin{aligned} T &= e^{\alpha t}\left[\frac{S_o}{\rho_F c_F \alpha} + A_1 \cosh\gamma_F x\right] && o < x < a \\ &= e^{\alpha t}\left[A_2 \cosh\gamma_A(b-x) + A_3 \sinh\gamma_A(b-x)\right] && a < x < b \\ &= e^{\alpha t}\, A_4\, e^{-\gamma_w(x-b)} && b < x \end{aligned}\right\} \quad (1)$$

where $\gamma^2 = \frac{\rho c}{k}\alpha$, $\alpha$ is the reciprocal exponential period, and the literal subscripts refer to fuel, aluminum cladding, and water. Analytic expressions for the constants, A, in terms of $\alpha$ and the k, $\rho$, c values of the three media can be obtained from the continuity conditions at the interfaces.[2]

For a fuel disc placed beside the core of the reactor, the heat source developed in the fuel will be proportional to the reactor power level at any time. Following the procedure introduced by Corben,[3] KEWB power traces can be represented empirically, up to the time of peak power, by the difference between two exponential functions and hence the heat source in the fuel can be represented by

$$S_{01}\, e^{\alpha_1 t} - S_{02}\, e^{\alpha_2 t}$$

where $\alpha_1$ and $\alpha_2$ are the two reciprocal exponential periods. A time and space temperature distribution for this source can be obtained by taking the difference of the solutions of Equations (1) for each individual component as was done by French.[4] The source constants for four typical KEWB power transients are given in Table I, and are applicable when the time origin is at the peak power of the experimental power trace.

TABLE I

| Nominal KEWB Period m.s. | Reciprocal Exponential Periods $sec^{-1}$ | | Source Strengths at Peak Power, 20% Enriched U in Fuel $cal\ cm^{-3}\ sec^{-1}$ | |
|---|---|---|---|---|
| | $\alpha_1$ | $\alpha_2$ | $S_{01}$ | $S_{02}$ |
| 1.02 | 800 | 2190 | $5.77 \times 10^5$ | $3.00 \times 10^5$ |
| 1.94 | 473 | 1150 | $1.88 \times 10^5$ | $0.846 \times 10^5$ |
| 5.23 | 183.3 | 368 | $0.461 \times 10^5$ | $0.239 \times 10^5$ |
| 8.42 | 111.3 | 223 | $0.236 \times 10^5$ | $0.1347 \times 10^5$ |

The constants were not chosen so that the time of peak power of the expression above necessarily matched that of the experimental power trace, but rather, so that the fit to the experimental curve was good over the few periods prior to peak power. For the values of $\alpha$ given in the table, the difference between the analytical and experimental power curves was never more than 5%. The values of $S_{01}$ and $S_{02}$ were obtained by normalization to an experimentally determined energy deposition

in the fuel disc. This experimental data has been obtained by Atomics International, using calorimetric methods in which the maximum temperature attained by a thermally insulated fuel disc was measured for a known energy release in the reactor core. The measurements were made with fuel discs of various enrichments and the results are given in Figure 4. The normalized values of $S_{01}$ and $S_{02}$ in Table I are for a U-Mo alloy fuel in which the uranium is 20% enriched.

Calculated temperature distributions existing at various times during a 1.94 millisecond KEWB transient are shown in Figure 5. The geometrical and thermal properties used in the calculation are given in Table II.

TABLE II

| Region | Fuel | Cladding | Coolant | Units |
|---|---|---|---|---|
| Material | U-Mo (U is 20% U235) | Aluminum | Water | |
| Thermal Conductivity | $2.9 \times 10^{-2}$ | 0.49 | 0.00147 | cal $cm^{-1}$ $^{o}C^{-1}sec^{-1}$ |
| Density | 17.3 | 2.7 | 1.00 | gm $cm^{-3}$ |
| Specific Heat | 0.040 | 0.230 | 1.00 | cal $gm^{-1}$ $^{o}C^{-1}$ |
| Thickness | 0.0508 | 0.010 | infinite | cm |

Similar calculations have been made to obtain temperature distributions that occur during transients having the other periods listed in Table I. A summary of all of the calculations

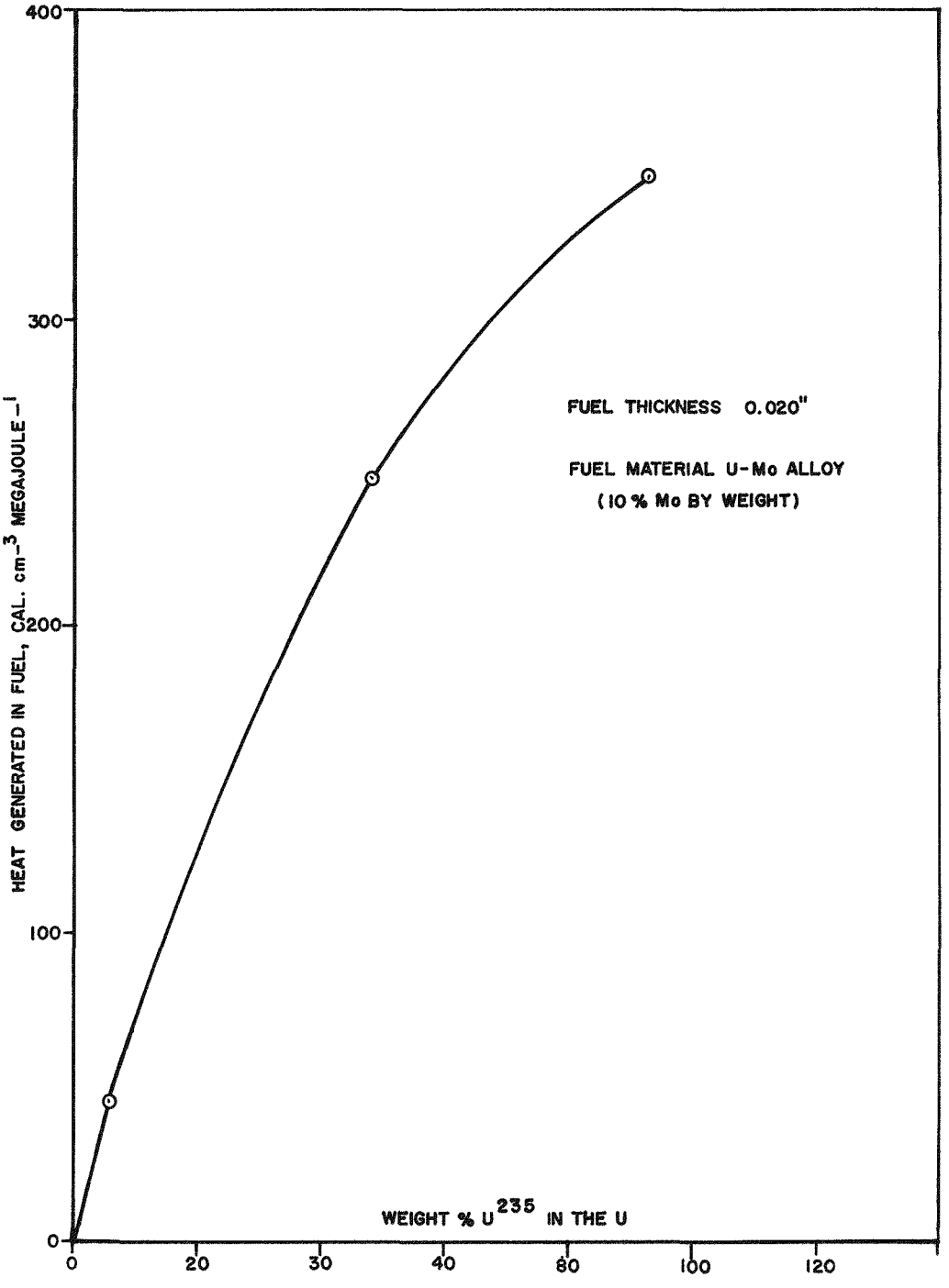


Figure 4. Energy Release Measurements for Fuel Discs Adjacent to the KEWB Reflected 18 Liter B Core (Atomics International Data).

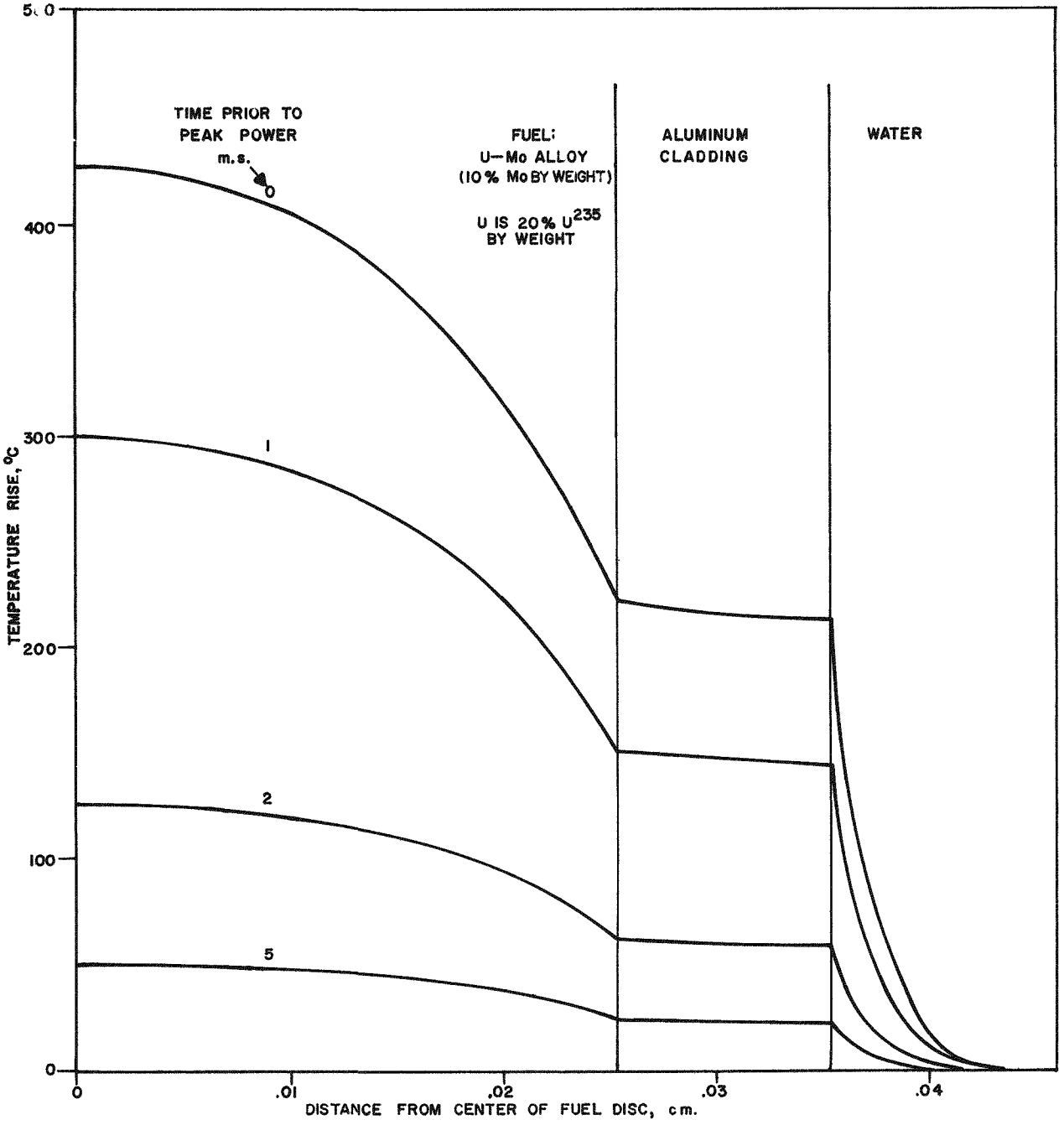


Figure 5. Calculated Temperature Distributions in the Fuel, Clad, and Water at Various Times Prior to Peak Power During a Transient with Initial Period of 1.94 ms.

at one spatial point, the interface of the water and the aluminum, is given in Figure 6. This set of curves has been normalized to apply to a fuel disc in which the uranium is 26% enriched (one of the fuel enrichments that will be available for use in the experiments). The upper curve in the figure is the limiting temperature that a thermally insulated disc would reach. A similar set of curves applicable to fuel discs of any other enrichment can be obtained by multiplying the ordinates in Figure 6 by a suitable factor determinable from Figure 4.

Although these calculations are only an approximation to the true temperature distributions that would exist, it is expected that they will be of use in making the rapid estimates needed to guide the course of the experiments. It should be mentioned that the geometrical arrangement of neutron absorbing and scattering materials around the fuel disc in the present experiments is somewhat different from the arrangement used during the insulated disc runs that formed the basis for the normalization. The calculations, when applied to the present experiments, therefore may be in error by some common fractional amount. It is estimated that this fraction may be as large as 30%, but the first series of measurements are expected to provide knowledge of the correct source strength.

More refined temperature and thermal expansion calculations will be required for interpretation of the experimental measurements, and for these computations a digital computer (IBM 7090) code has been prepared. It provides a solution of the heat equation, for the one dimensional three region problem, in which account is taken of the temperature dependence of the conductivities, densities, and specific heats of the three materials. The heat source in the fuel can have an arbitrary time dependence and an arbitrary, but separate, space dependence. Hence a

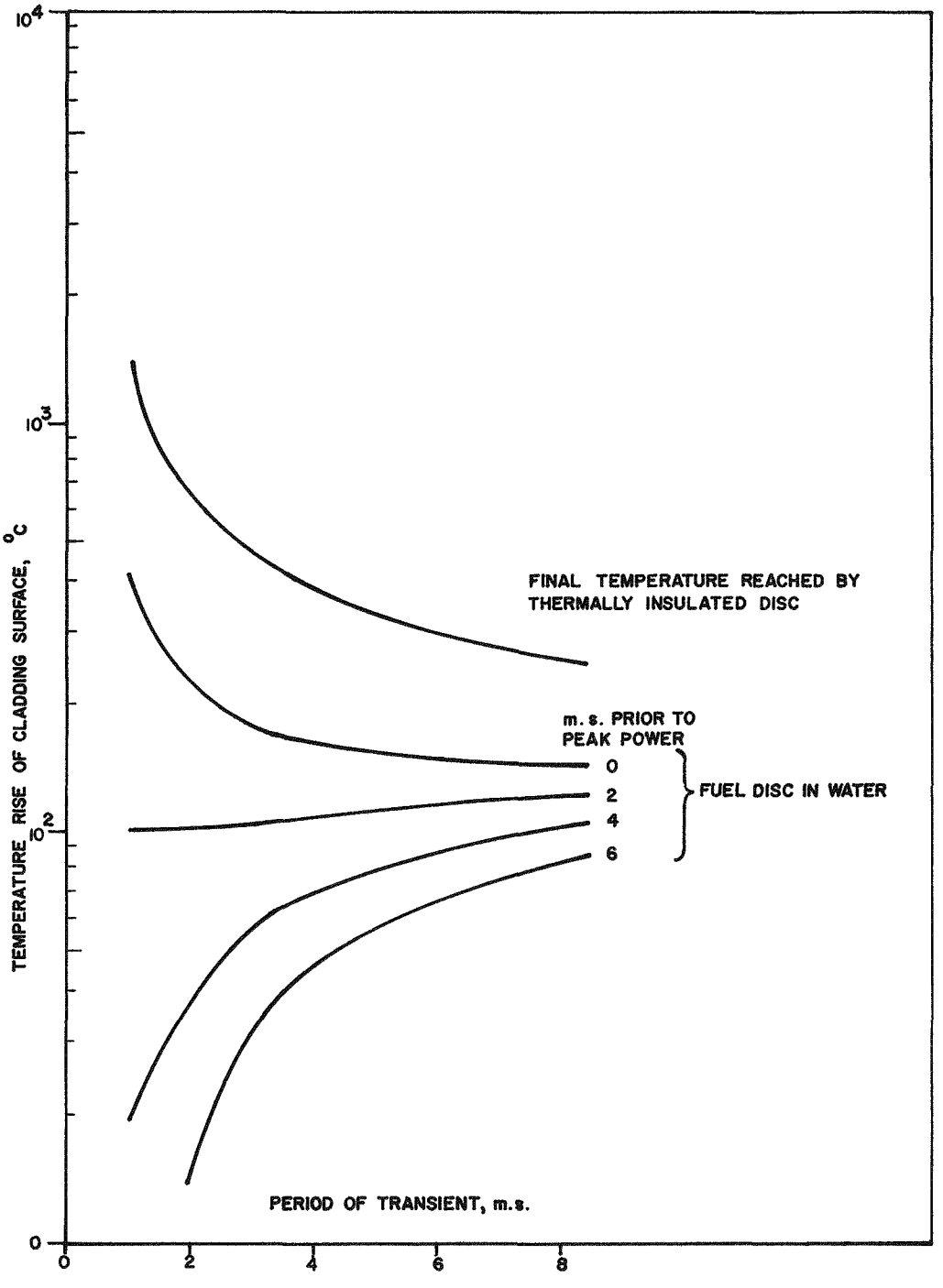


Figure 6. Calculated Surface Temperature Rise for Various Time Intervals Prior to Peak Power, as a Function of KEWB Initial Period. Calculations are for a U-10 Mo Disc with 26% Enrichment ($U^{235}$).

realistic source function can be introduced which is proportional to an experimentally observed reactor power history and has a spatial shape in the fuel that is determined from the thermal neutron absorption. The source can be normalized by bringing the calculated temperature at the aluminum surface into agreement with the measured temperature at some selected time.

## III. PRESSURE TRANSIENT EXPERIMENT (R. W. Wright)

A mechanism was proposed in our March 1962 quarterly report to explain the large pressure pulse (about 8,000 psi) which occurred in the BORAX I destructive power excursion[1,5]. During the present quarter, design and construction were nearly completed upon an experiment to test this hypothesized mechanism for the occurrence of large pressure pulses during rapid power excursions in heterogeneous water reactors. The large pressure pulses are attributed to the very rapid thermal expansion of the layer of water a few microns thick which is in contact with the fuel plates as the plate surface temperature rises rapidly through the thermodynamic critical temperature of water. The inertial loading of the surrounding water converts this sudden expansion into a large pressure pulse. The rapid thermal expansion occurs because of the very large bulk expansion coefficient of water (or expansivity) slightly above the critical temperature. An approximate analysis of the magnitude of the pressure pulse to be expected from this effect in the BORAX I destructive power excursion is given in our March quarterly[1]. The calculated peak pressure was about 4,000 psi. This is in excess of the critical pressure of water, 3,200 psi, and demonstrates that this mechanism can produce greater than critical pressure pulses. In view of the approximate nature of the calculations, the agreement with the magnitude of the BORAX I destructive pulse of 6,000 to 10,000 psi is considered satisfactory.

Three conditions appear to be necessary in order for these large pressures to occur. First, the fuel plate surface temperature must pass through the water critical temperature with a sufficiently large time rate of temperature rise. Second, the ratio of effective heated fuel surface area to area available for pressure relief must be sufficiently large. Third, a sufficient inertial head of water must be present.

In this experiment, a thin-walled stainless steel tube is heated by a short electrical pulse (150 μsec long). The resulting transient water pressure inside the rigid capsule enclosing the tube is measured for different temperature increments applied to the heated tube. The temperature increment, from a room temperature start, will be increased in steps to well above the critical temperature of water. The hypothesized mechanism will have been verified if a large pressure pulse occurs with a sharp threshold in the temperature increment. This threshold should be well above the actual water critical temperature as will be explained later.

A schematic drawing of the mechanical apparatus is shown in Figure 7. The heated element is a .002" thick stainless steel tube 1/4" in diameter and 2" long, with thicker end rings for mechanical support and electrical connection. A .060" diameter copper rod along the axis of the tube furnishes a coaxial current return so that the magnetic pressure on the tube will be radially outward with zero net magnetic force on the tube. The tube and rod are mounted coaxially in a 3/8" diameter water filled cavity in a heavy rigid stainless steel block, one side of which can be removed for assembly. In the bottom of the cavity, just below the heated element, a small ceramic piezoelectric crystal is mounted coaxially for transient pressure measurements. Extending vertically upward from the block is a 3 foot long pipe which extends the water cavity in order to furnish an inertial head of water above the heated element corresponding to that in BORAX I. Surface heating elements are fastened to the outside of the block and tube so that the initial water temperature may be above room temperature, or above 100°C if pressurization is used. The structure is designed to withstand pressures of 10,000 psi. The experimental apparatus is shown disassembled in Figure 8. The heated element is mounted on the removable section

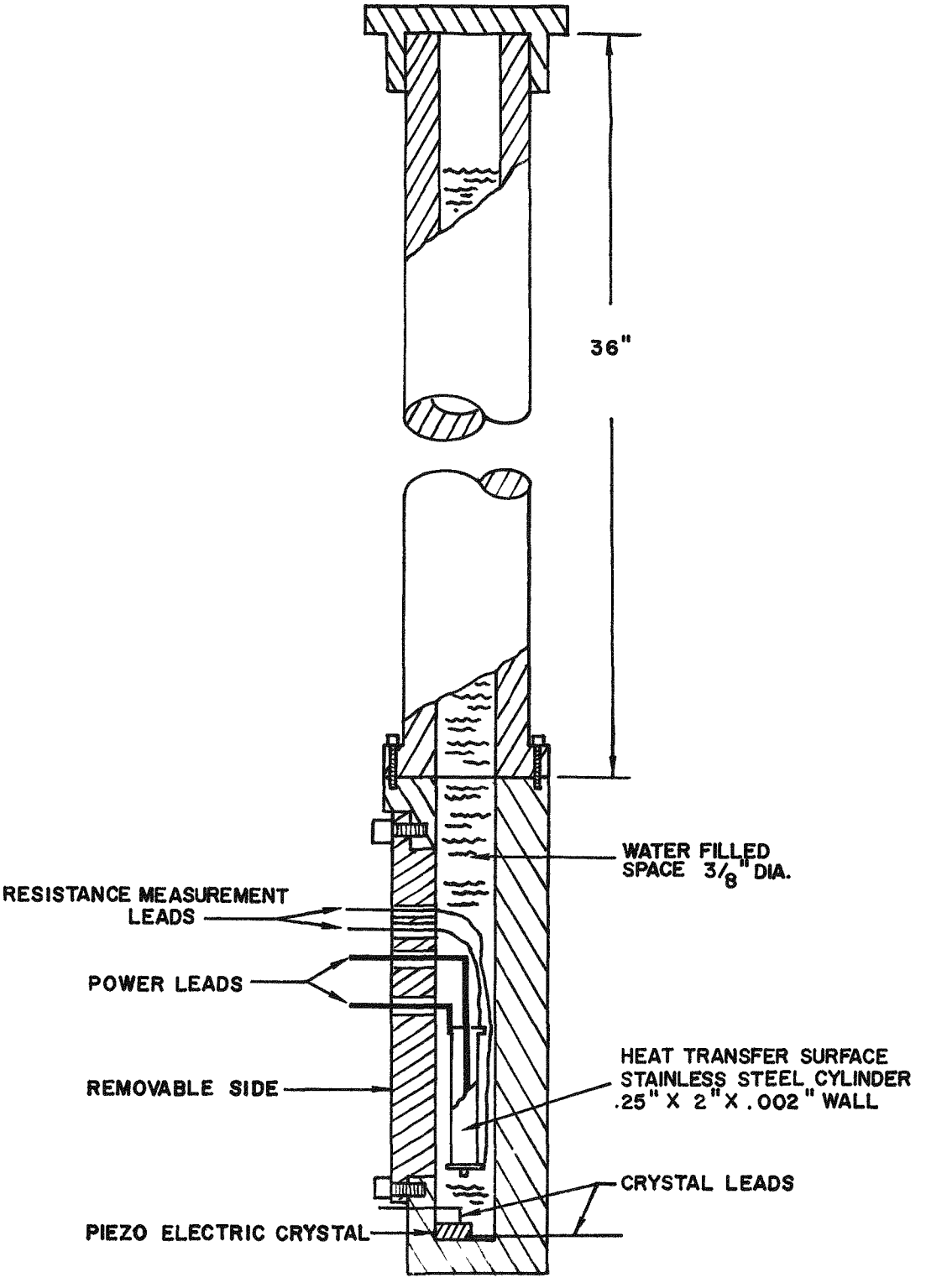


Figure 7. Conceptual Design of the Mechanical Apparatus (Pressure Capsule) for the Out-of-Pile Measurement of Extreme Pressure Transients.

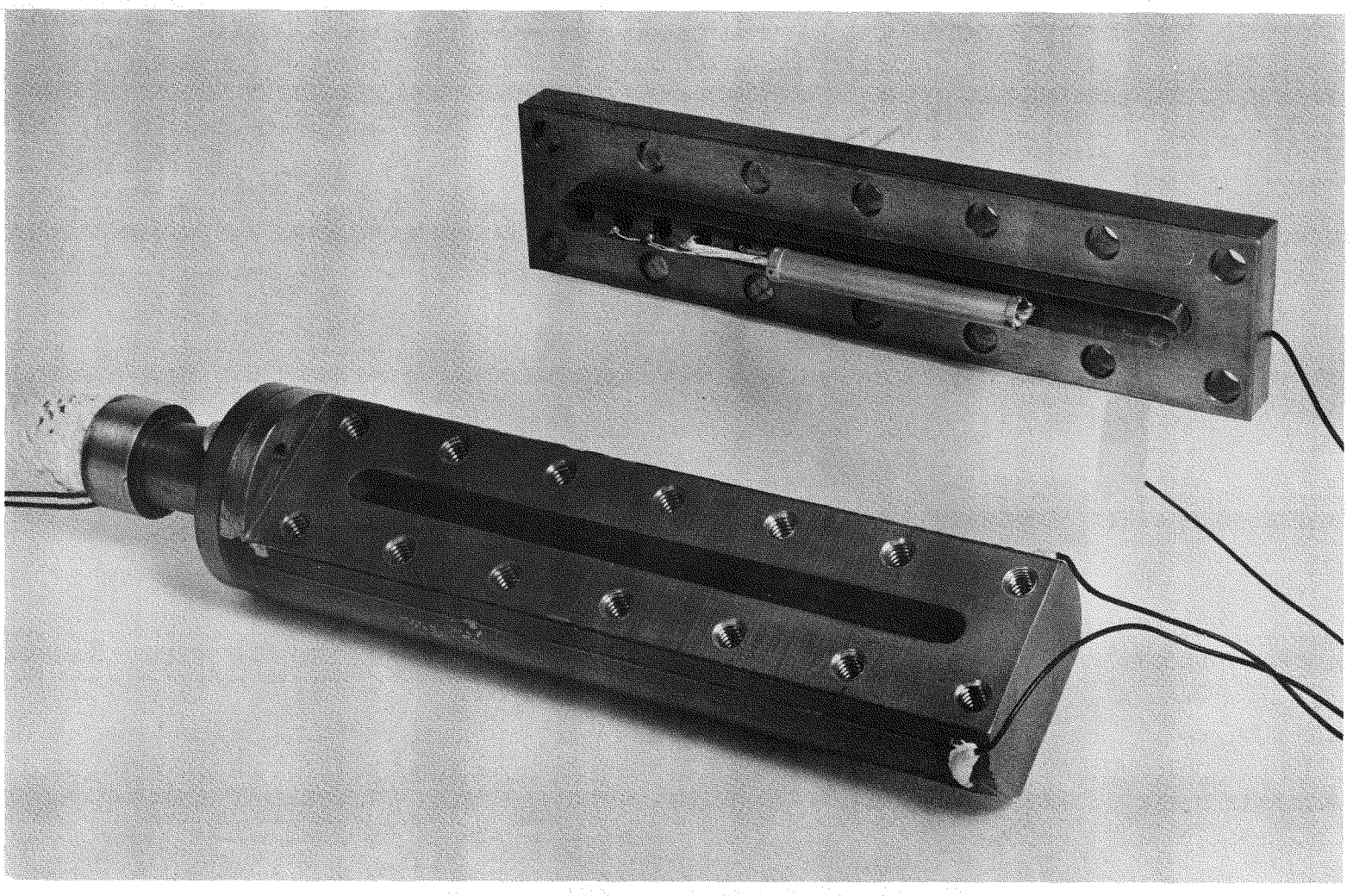

Figure 8. Disassembled Pressure Capsule.

of the heavy block. The heavy wires are for the external heating elements. A close-up view of the removable section with the heated element and associated wiring attached is shown in Figure 9. The two fine wires coming from the heated element are for measuring the element's temperature following the heating pulse by means of resistance measurement.

The heated surface area is 30 times the area available for pressure relief which is the 3/8 inch diameter cross section of the water cavity. (The stainless steel walls of the cavity are essentially rigid.) The corresponding ratio used in the calculations in Reference 1 of the BORAX I destructive transient was 18, so this experiment should have a sufficiently small pressure relief area to produce the hypothesized pressure pulse. The inertial water head, which calculations have shown not to be critical, is also similar to the BORAX I case.

Water Temperature History - During the exponential portion of the BORAX I destructive power excursion (2.5 ms period) the rate of temperature increase of each element of water as it passed through the water critical temperature (374°C) was $1.4 \times 10^5$ °C/sec. Reproducing the reactor's exponentially increasing power on a 2.5 ms period did not appear feasible with electrical heating. Instead a short rectangular pulse of electrical power is applied to the heated stainless tube. This pulse has sufficient magnitude to produce the desired rate of temperature rise in elements of water a few microns from the heated surface as they pass through the thermodynamic critical temperature of water.

An idealization of this process is the application of a step temperature increase to the heated surface. A one dimensional calculation is accurate for distances a few microns from the cylindrical heated surface which has a radius of

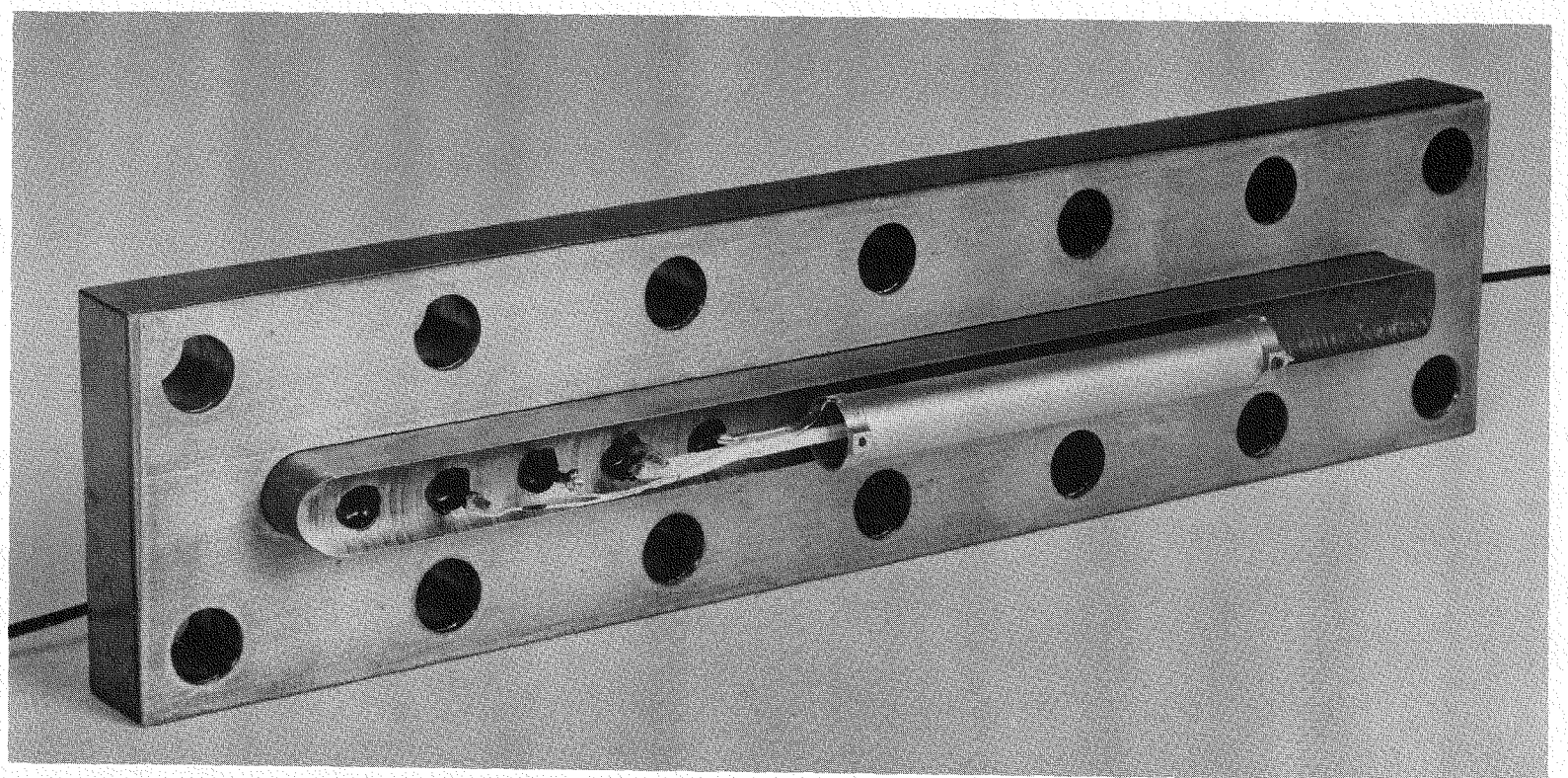

Figure 9. Removable Section of Pressure Capsule Showing Cylindrical Heating Element and Associated Wiring.

curvature of 3,200 μ. The temperature rise θ in the water at time t after a step of unit magnitude at a distance x from the heated surface is:[6]

$$\theta = 1 - \frac{2}{\sqrt{\pi}} \int_0^{\frac{x}{2\sqrt{\alpha t}}} e^{-z^2} \, dz$$

where the thermal diffusivity $\alpha = 1.3 \times 10^{-3}$ $cm^2/sec$ for water. The rate of temperature rise is:

$$\frac{d\theta}{dt} = \frac{x}{2\sqrt{\pi \alpha t^3}} e^{-x^2/4\alpha t}$$

Figure 10 is a graph as a function of time of θ and dθ/dt at a plane in the water 10 μ from the heated surface. The temperature step is equivalent to a delta function (spike) heat input to the heated element because the heat loss into the water is negligible for these short times.

Figure 10 shows that the maximum rate of temperature rise for a step input occurs when the temperature has risen to only 8% of the final temperature, and that the rate of rise falls off steadily thereafter as the water slowly approaches the final temperature. This is true at all distances into the water, and is only slightly modified at the 10 μ depth for a 150 μsec heating pulse. To achieve a rapid rate of temperature rise in an element of water as it passes through its critical temperature it is therefore necessary to pulse the heated surface to well above the critical temperature. A temperature rise of about 350°C is required to raise water from room

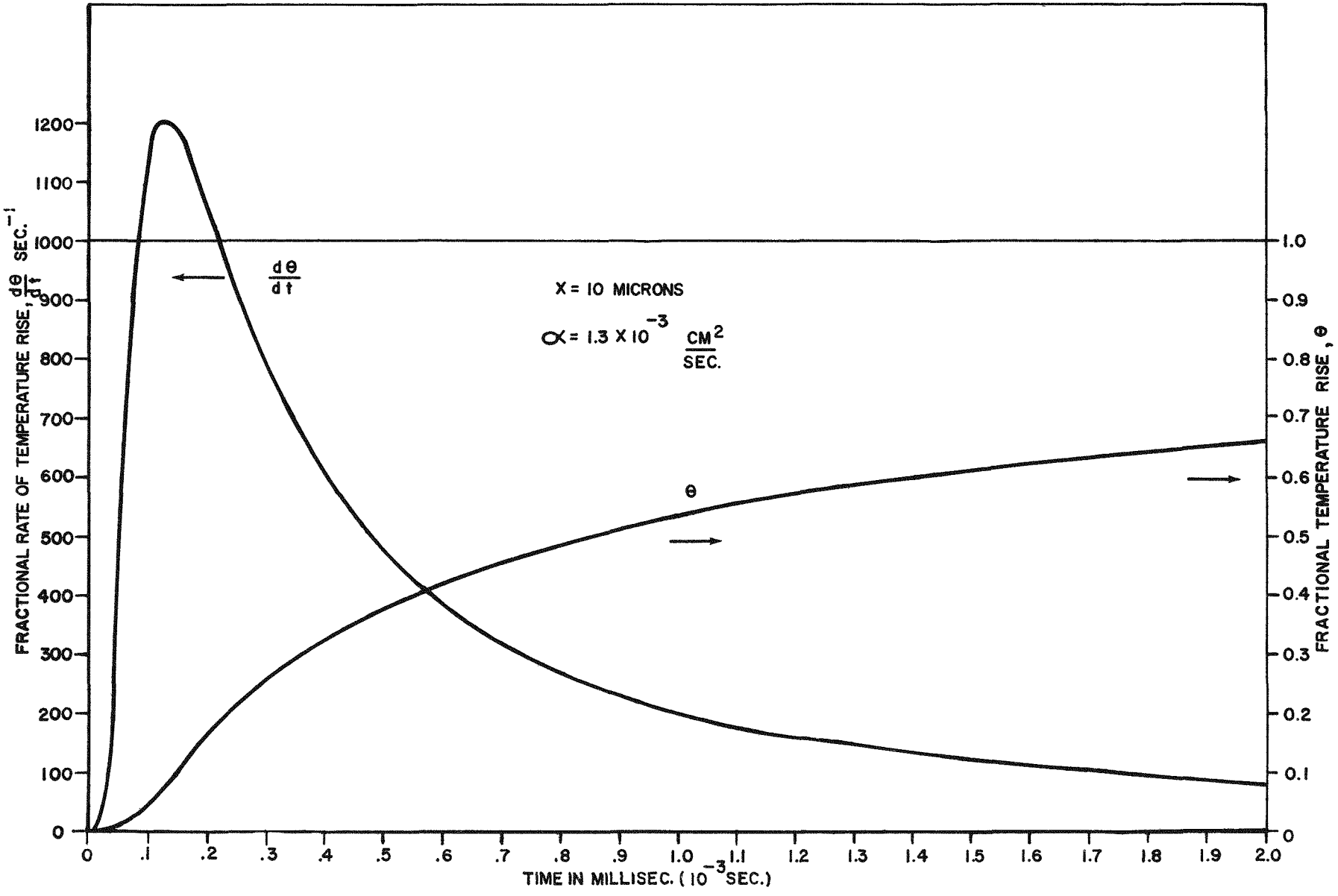


Figure 10. Fractional Temperature Rise and Rate of Rise 10 Microns into a Semi-Infinite Slab of Water Following an Applied Unit Temperature Step. Diffusivity of $1.3 \times 10^{-3}$ $cm^2/sec$ Assumed Throughout.

temperature to its critical point of 374°C. For this experiment a nominal design temperature rise of 700°C was chosen, about twice the rise necessary to reach the critical temperature of water. Figure 10 shows that, for a 700°C temperature step from room temperature, the rate of temperature rise will be 21% of the maximum when elements of water pass through the critical temperature. At 10 μ depth, the water critical temperature will be reached 840 μsec after the step with a rate of rise of $1.8 \times 10^5$ °C/sec. This is to be compared with the BORAX I rate of rise of $1.4 \times 10^5$ °C/sec for water passing the critical temperature. For smaller depths x into the water, the rate of rise at the critical temperature will be increased by the factor $(10/x)^2$ where x is in microns, and will occur at times reduced by $(x/10)^2$. As the calculations in Reference 1 were made for the 5 μ layer of water next to a fuel plate, this experiment is capable of exceeding the rate of temperature rise used in these calculations as well as the rate of rise of the 10 μ thick layer of water adjoining the fuel plates in the BORAX I destructive experiment.

A heating pulse length of 150 μsec was chosen as a compromise between difficulties with the high powers required for short pulses and the desirability of terminating the electrical interference from the heating pulse before pressure pulses of interest may occur. The finite pulse length "smears" the curves of Figure 10 by 150 μsec. This is shown in Figure 11 where θ and dθ/dt are plotted as functions of time from the start of the 150 μsec rectangular pulse at planes 0 μ and 10 μ into the water. The average effective values of θ and dθ/dt for pressure pulse production in this experiment should lie between the curves for 0 and 10 μ, so use of the 10 μ curve for heating requirements is conservative. When the 150 μsec length of the 700°C heating pulse is taken into account, as in Figure 11, an

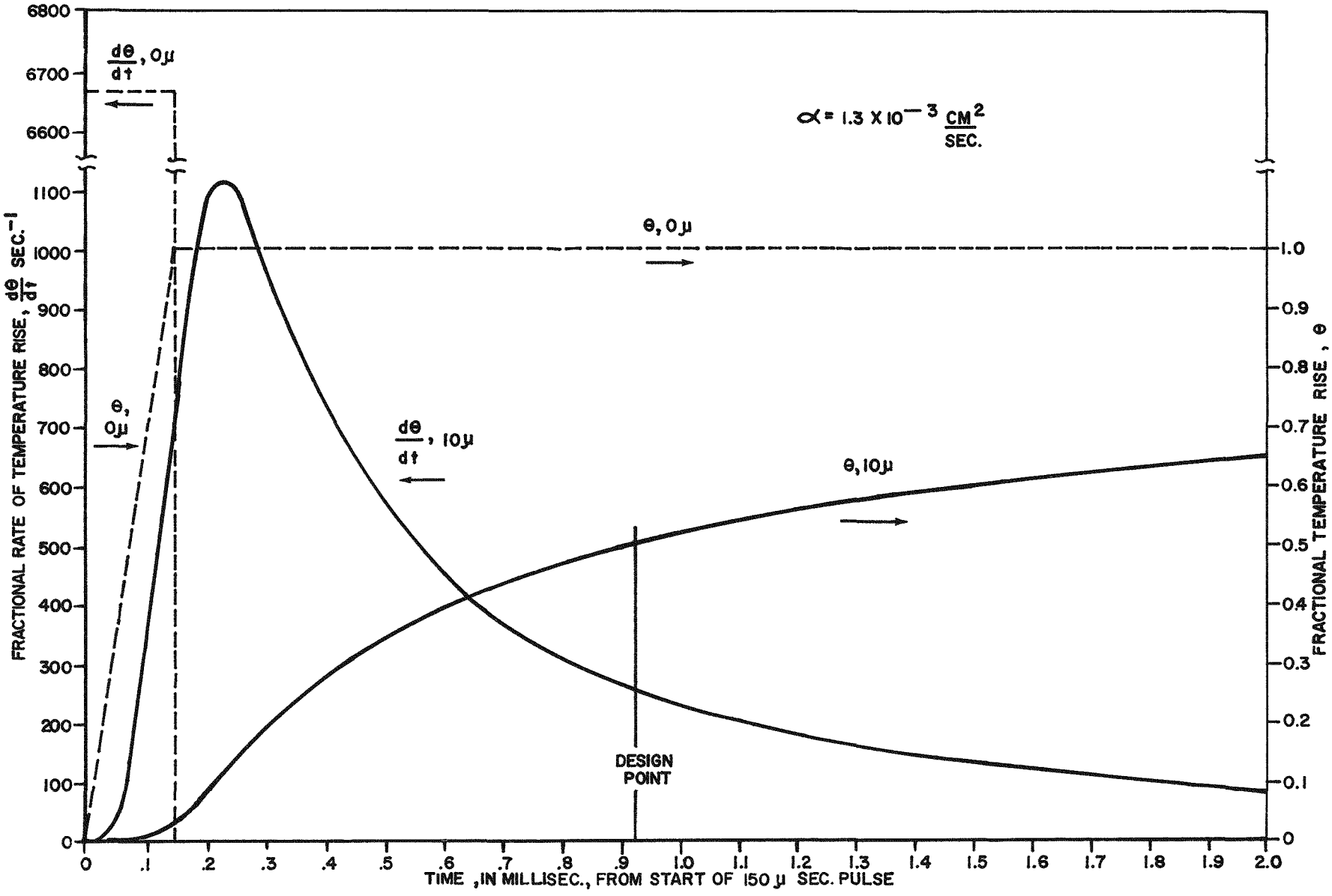


Figure 11. Fractional Temperature Rise and Rate of Rise 0 Microns and 10 Microns into Semi-Infinite Slab of Water After the Start of Application of a Unit Temperature Rise in 150 μsec. Diffusivity of $1.3 \times 10^{-3}$ $cm^2/sec$ Assumed Throughout.

element of water 10 μ from the heated surface will pass through the critical temperature 910 μsec after the start of the pulse with essentially the same $1.8 \times 10^5$ °C/sec rate of temperature rise as for a 700°C step.

The time of occurrence of these hypothesized large pressure pulses is determined by the "effective depth" in the water at which they are generated. For a 700°C temperature increment, water less than 4 μ from the surface will have passed the critical temperature by the end of a 150 μsec pulse. This water will have a greater rate of temperature rise than water at 10 μ will experience. If it becomes necessary, in order to measure the pressure signal, the electrical system could probably produce 50 μsec pulses at 3 times design power, but the mechanical strength of the connecting wires inside the capsule might not be adequate. The rate of temperature rise at the critical point can also be increased considerably by pre-heating the capsule and water so that the critical temperature is reached sooner. For example, at 10 μ depth, initial water temperature of 150°C, and with a 700°C applied temperature increment, the rate of temperature rise at the critical point is increased to $4.2 \times 10^5$ °C/sec from the $1.8 \times 10^5$ °C/sec obtained with a room temperature start. Electrical heating elements are provided on the external surface of the capsule and on the static head tube for this pre-heating, and the capsule may be pressurized to permit initial temperatures above 100°C. We do not expect that this initial heating will be required.

Electrical System - The electrical heating system is designed to raise the temperature of the .002" thick, 1/4" diameter, 2" long stainless steel tube 700°C in 150 μsec. This is twice the temperature rise necessary to reach the critical temperature of water from room temperature. A nominally rectangular 1 Mw pulse of electrical power is applied for 150 μsec

to do this. The energy is stored in a three section artificial transmission line of 1200 μf total capacitance and 4.5 μh total inductance. The line has a characteristic impedance of 0.06 Ω. It matches the 0.05 Ω resistance of the heating element with an allowance for 20% loss. The matching is done in order to produce a relatively rectangular current pulse with a fairly sharp termination. The latter is necessary in order that the piezoelectric pressure signal can be observed a few hundred microseconds after the beginning of the heating pulse without being masked by electrical pickup from the large electrical heating current. The design heating current of 4,600 amps is obtained when the line is charged to 550 volts. Smaller temperature increments are obtained by reducing the voltage to which the line is charged. A General Electric GL-7703 ignitron is used to discharge the line through the load.

The piezoelectric pressure transducer is a Clevite PZT-4 ceramic disc, 1/4 inch in diameter and 0.1 inch thick. It is loaded with 0.01 μf parallel capacitance to reduce the output voltage and impedance.

Following the heating pulse, the temperature of the heating element will be measured by connecting it rapidly to an unbalanced Kelvin double bridge circuit and measuring the resistance. A large pressure pulse would probably break the fine wires attached to the heating element for resistance measurements. These measurements, therefore, will only be used in relatively low power tests to determine the electrical efficiency for transfer of stored energy from the capacitors to the heated element. This efficiency can then be used with the measured stored electrical energy to calculate the temperature rise of the heating element in the high power tests, even if the heating element is destroyed.

## PART IV. AN ANALYSIS OF THE HYDRODYNAMIC STABILITY OF PARALLEL CHANNELS IN A NATURAL CIRCULATION BOILING WATER REACTOR (G.C.K. Yeh and S.M. Zivi)

The subject of hydrodynamic oscillations in single channel flow loops was reviewed in our June quarterly. The analysis presented in the following is directed toward the prediction of hydrodynamic oscillations in a system of many parallel channels, utilizing experimental information obtained in the laboratory on a single boiling channel. This analysis was undertaken on an exploratory basis and some of the tentative assumptions are made primarily to reduce the algebraic complexity. In particular, it is assumed that the system consists of (n) parallel channels which are identical, and which are arranged symmetrically with respect to a common downcomer. It is also assumed that the system operates at the peak natural circulation flow rate. These assumptions are not essential to the analysis and the results obtained thus far provide considerable incentive to continue the analysis with less restrictive assumptions.

Two other assumptions are required by the present lack of knowledge of detailed mechanisms of two-phase flow dynamics. First, it is assumed that the steam quality in the two-phase mixture leaving the boiling channels is small (say no greater than 10%). This enables us to write an approximate equation of continuity without introducing some arbitrary assumption on the slip ratio (the ratio of vapor velocity to liquid velocity). Secondly, it is assumed that the periods of oscillation are much lower than the residence time of the two-phase fluid in the boiling region of each channel. This assumption enables us to consider the pressure disturbances in the boiling region of each channel to be propagated essentially instantaneously throughout the boiling region.

The other major assumption is that the system disturbances are small in amplitude so that linear approximations are valid.

The assumption that the steady-state quality of the two-phase mixture leaving each channel is small, enables us to write a continuity equation which considers only the liquid flow at each channel inlet and exit, together with changes in the steam void volume within each channel. Eq. 2 is the continuity equation for the J-th channel in the system illustrated schematically in Figure 12.

$$\frac{d}{dt} V_J = E_J - F_J;\ J = 1, 2, \ldots . n \qquad (2)$$

where

$V_J$ = steam void volume in the J-th channel

$E_J$ = exit liquid volumetric flow rate, the J-th channel

$F_J$ = inlet liquid volumetric flow rate, the J-th channel

$t$ = time

$n$ = total number of channels

If we consider only sinusoidal variations about the mean values of the variables, Eq. 2 may be expressed as follows:

$$j\omega\delta V_J = \delta E_J - \delta F_J \qquad (3)$$

where

$\delta V_J$ = sinusoidal variation of steam void volume from the mean value

$= \bar{V}_J\, e^{j\omega t}$

$j = \sqrt{-1}$

$\omega$ = frequency of sinusoidal disturbance, radians/sec

$\delta E_J$ = sinusoidal disturbance in exit liquid flow rate.

$\delta F_J$ = sinusoidal disturbance in inlet liquid flow rate.

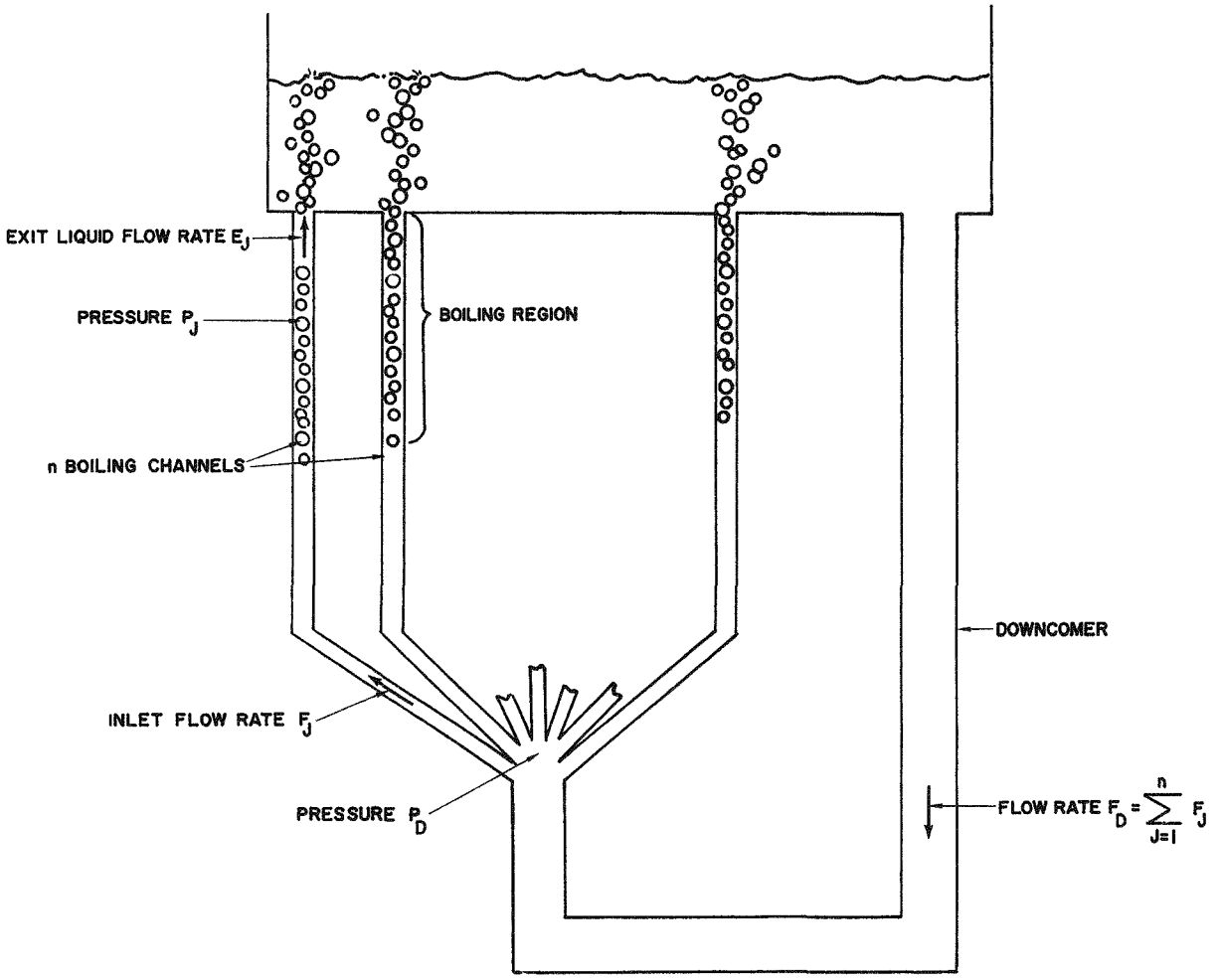


Figure 12. Schematic Diagram of the Multi-Channel System for Hydrodynamic Stability Analysis.

Another continuity equation must be written at the point where the (n) channels meet the downcomer (see Figure 12.,

$$\delta F_D = \sum_{J=1}^{n} \delta F_J \qquad (4)$$

where

$\delta F_D$ = flow disturbance in the downcomer.

We now apply the impedance concept used in our previous transfer function analysis[7] where the impedance is defined as the ratio of the local pressure disturbance to the local flow disturbance,

$$Z_D = \frac{\delta P_D}{\delta F_D} \qquad (5)$$

$$Z_E = \frac{\delta P_J}{\delta E_J}$$

$$Z_I = \frac{\delta P_J - \delta P_D}{\delta F_J}$$

where

$Z_D$ = Downcomer impedance.

$Z_E$ = Channel exit impedance, assumed identical for all (n) channels.

$Z_I$ = Channel inlet impedance, assumed identical for all (n) channels.

$\delta P_J$ = Pressure disturbance in the two-phase region of the J-th channel.

$\delta P_D$ = Pressure disturbance at the base of the downcomer.

The locations of the pressure disturbances in Eq. 5 are indicated in Figure 12. Utilizing the assumption that pressure disturbances occur uniformly throughout the two-phase region of each channel, and applying Eq. 5, we have the following:

$$\delta P_J = Z_E \delta E_J = Z_I \delta F_J + Z_D \delta F_D \qquad (6)$$

Rearranging and substituting Eqs. 3 and 4 results in

$$\delta F_J (Z_E - Z_I) + j\omega Z_E \delta V_J = Z_D \sum_{i=1}^{n} \delta F_i \qquad (7)$$

At this point, it is convenient to introduce the symbol $H_{VF}$, the void-flow transfer function as defined by

$$H_{VF} = \frac{\delta F_J}{\delta V_J}$$

where

$$H_{VF} = \text{void-flow transfer function for J-th channel (assumed identical for all (n) channels).} \qquad (8)$$

The assumption that all channels are identical and symmetrical means that $H_{VF}$ will be the same for all (n) channels. Substituting Eq. 8 into Eq. 7, we obtain the expression

$$\delta F_J \left(Z_E - Z_I + j\omega \frac{Z_E}{H_{VF}}\right) = Z_D \sum_{i=1}^{n} \delta F_i \qquad (9)$$

which is of the form

$$x_i B = C \sum_{i=1}^{n} X_i \qquad (10)$$

$$x_2 B = C \sum_{i=1}^{n} x_i \qquad \text{(10,cont)}$$

.....

$$x_n B = C \sum_{i=1}^{n} x_i$$

when all (n) channels are considered simultaneously. There are only two possible solutions to the system Eq. 10, namely

$$\left.\begin{aligned} x_1 &= x_2 = \ldots = x_n \\ B &= Cn \end{aligned}\right\} \qquad (11)$$

or

$$\left.\begin{aligned} \sum_{i=1}^{n} x_i &= 0 \\ B &= 0 \end{aligned}\right\} \qquad (12)$$

This result means that Eq. 9 has two possible solutions,

$$\left.\begin{aligned} \delta F_1 &= \delta F_2 = \ldots = \delta F_n \\ Z_E - Z_I + j\omega \frac{Z_E}{H_{VF}} &= nZ_D \end{aligned}\right\} \qquad (13)$$

or

$$\left.\begin{aligned} &\sum_{i=1}^{n} \delta F_i = 0 \\ &Z_E - Z_I + j\omega \frac{Z_E}{H_{VF}} = 0 \end{aligned}\right\} \qquad (14)$$

Each of Eq. 13 and 14 describes a void-flow transfer function $H_{VF}$ for the possible modes of oscillation. The first mode as given in Eq. 13 has all channels oscillating in phase with each other*, and the second mode as given in Eq. 14 represents out-of-phase oscillations in which there is complete accomodation of the flow disturbances by the interactions of the parallel channels, and consequently there is zero net flow disturbance in the downcomer. This second mode of motion is identical to the oscillations which may arise in a forced circulation system where the total flow rate is constrained to a constant value.

The criteria for hydrodynamic stability are developed in the following. In our earlier studies [7, 8] a feedback model for hydrodynamic instabilities was introduced. This same model is useful in appraising parallel channel stability. In the model, it is recognized that a flow disturbance will produce a disturbance in the steam void volume in a boiling channel, and this effect is described as a flow-void transfer function, $G_{FV}$, which is defined by

$$G_{FV} = \frac{\delta V_J}{\delta F_J} \qquad (15)$$

---

*Thereby being identical to a single channel oscillation in a simple laboratory loop.

Eq. 15 and 8 are independent; each represents a distinctly different physical phenomenon. Eq. 8 defines the flow rate disturbance which would ensue as a result of an imposed void-volume disturbance, whereas Eq. 15 describes the void volume response to an imposed inlet flow rate disturbance. $H_{VF}$ is defined by Eq. 13 or Eq. 14 (depending upon the mode of motion being considered), whereas $G_{FV}$ can be measured by modulating the flow rate in a boiling channel and measuring the void fraction response. These measurements are being prepared in our laboratory and also at Argonne National Laboratory[9]. Meanwhile, an estimate of the flow void transfer function ($G_{FV}$) can be obtained from transfer function measurements which we have performed on a channel of SPERT IA dimensions at 1 atm pressure and at 500 watts power. Two sets of measurements were made, the first with natural circulation and the second with forced circulation at the same mean flow rate. The vector difference between the two void fraction responses, divided by the measured flow response in the natural circulation case, yields the flow void transfer function for these operating conditions. The results of this measurement are given in Figure 13 and Figure 14*. The data in these figures are considered only approximate because of the inherent inaccuracy in the vector subtraction process.

It is possible to apply the Nyquist criterion to determine the hydrodynamic stability of this system. Referring to Figure 15, where the feedback loop is shown for an externally imposed void volume disturbance to the system, we find that the Nyquist criterion would predict a hydrodynamic instability when the locus of the quantity ($-H_{VF}G_{FV}$) encircles the -1 point in the complex plane. As an illustration of the application of this analysis, we have plotted the Nyquist diagram for a system of

---

*It will be noted that the amplitude of $G_{FV}$ given in Figure 13 is changed from that given in Ref. 7, Figure 30. This is the result of the correction of an error in Ref. 7. The phase shift shown in Figure 14 differs from the corresponding quantity in Ref. 7, Figure 31 for the same reason.

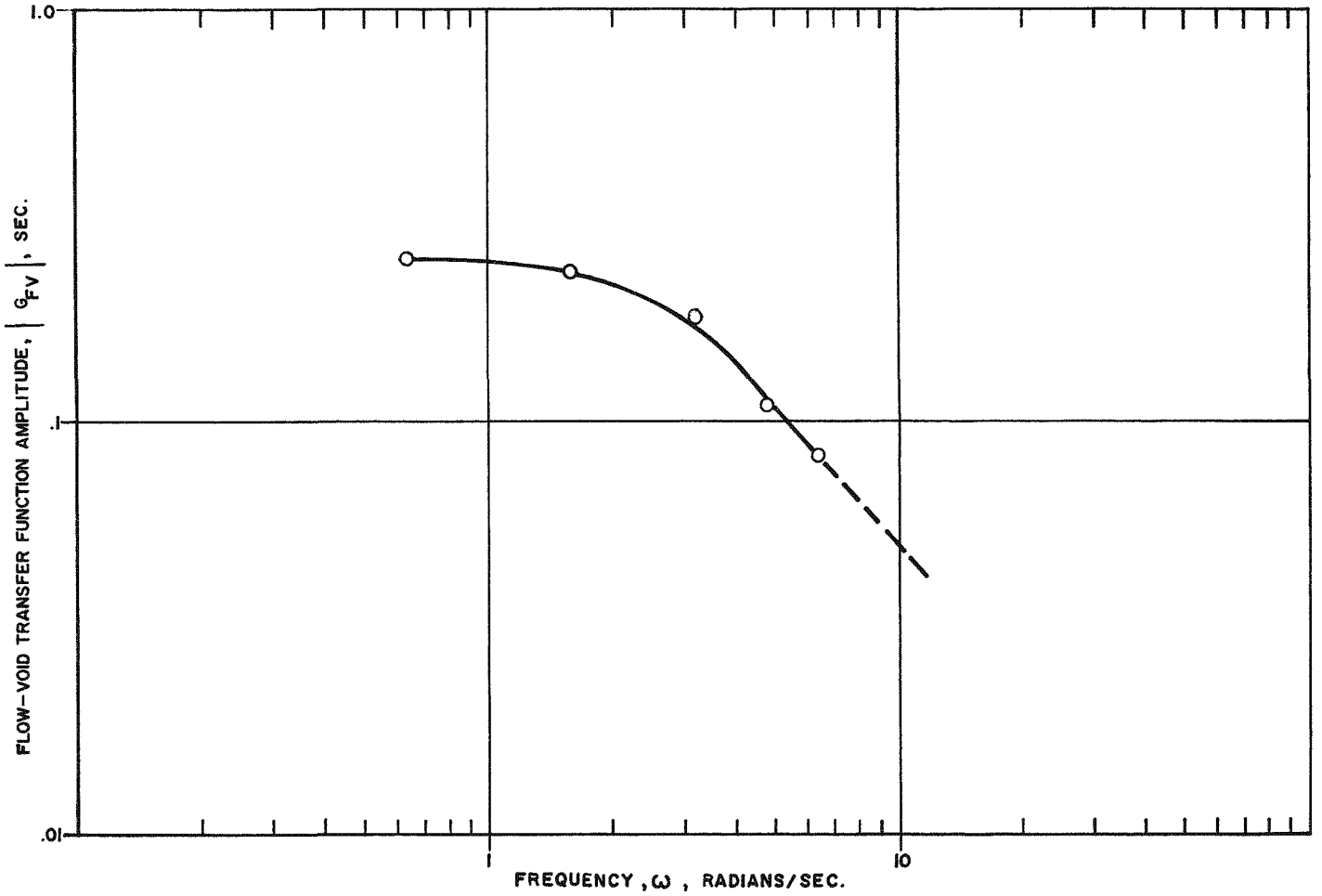


Figure 13. Approximate Amplitude of the Flow-Void Transfer Function ($G_{FV}$) for a SPERT IA Channel at 500 Watts Power, 44.5 cm/sec Mean Inlet Velocity, 100°C Inlet Water Temperature, 2 Ft. Hydrostatic Head Above Channel Exit. These data were obtained from the difference between two measurements of void fraction response to power modulation. One set of measurements was taken with the experimental loop operating in natural circulation, with a measured inlet flow response. The second set of measurements was taken with forced circulation, and hence, zero inlet flow modulation.

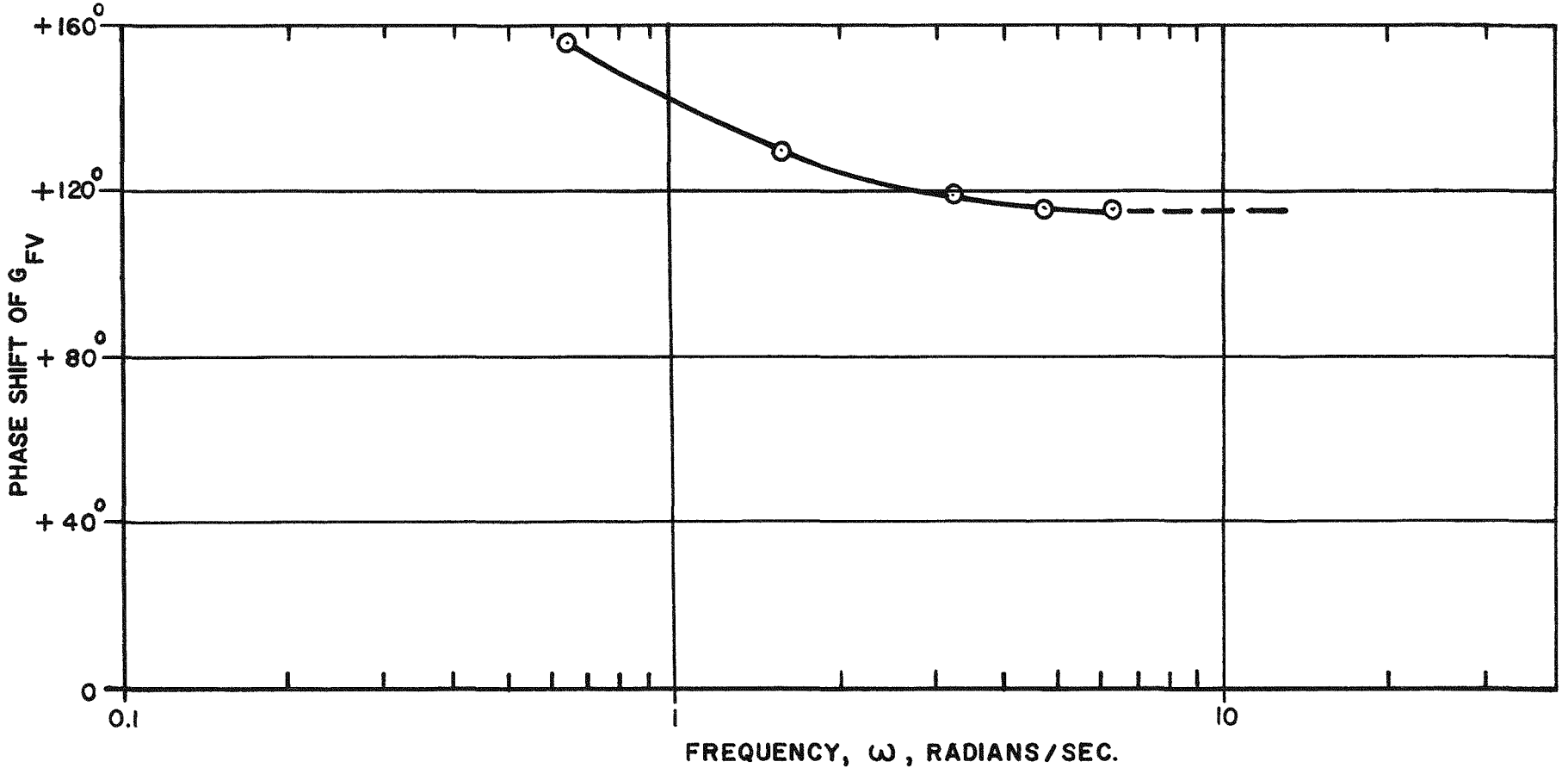


Figure 14. Approximate Phase Shift of the Flow-Void Transfer Function ($G_{FV}$) for a SPERT IA Channel. Conditions as in Figure 13.

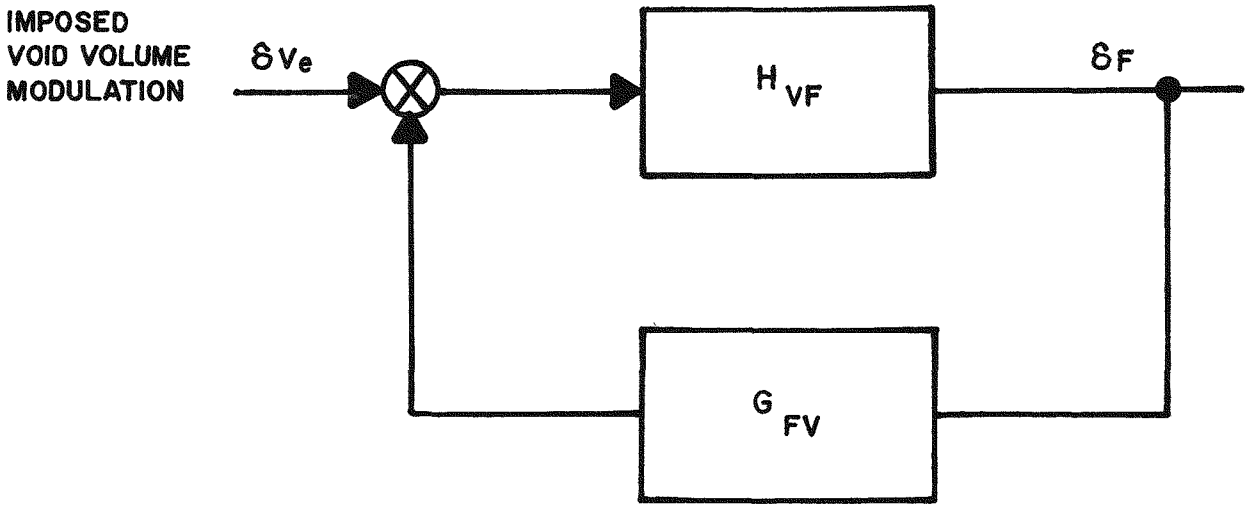


$$\frac{\delta F}{\delta V_e} = \frac{H_{VF}}{1 - H_{VF}\ G_{FV}}$$

Figure 15. Flow-Void Feedback Loop Relevant to Linear Hydrodynamic Instabilities (for operation at the peak natural circulation flow rate.

SPERT IA channels, each operating at 500 watts power, at 1 atm, with a mean inlet water velocity of 44.5 cm sec, and a constant inlet water temperature of 100°C. The results are independent of the number of parallel channels, assuming that when (n) single channels are combined into a parallel channel system, the total downcomer cross-sectional area would equal (n) times the downcomer area which would be provided for a single channel. That is, if $Z_{SD}$ is the downcomer impedance in the single channel loop experiment in which $G_{FV}$ is measured, then the multiple channel downcomer impedance $Z_D$ would be given by

$$Z_D = \frac{1}{n} Z_{SD} \tag{16}$$

where

$Z_D$ = downcomer impedance for system of (n) parallel channels.

$Z_{SD}$ = downcomer impedance for single channel system.

Substituting Eq. 16 into Eq. 13, we find that we have eliminated the dependance on (n). This is shown in Eq. 17, which includes the substitution and a rearrangement.

$$H_{VF} = \frac{j\omega}{\frac{Z_{SD}+Z_I}{Z_E} - 1} \quad \text{for all channels oscillating in phase with each other.} \tag{17}$$

We also rearrange Eq. 14 to obtain the other expression for $H_{VF}$

$$H_{VF} = \frac{j\omega}{\frac{Z_I}{Z_E} - 1} \quad \text{for parallel channel flow oscillations cancelling each other.} \tag{18}$$

The results of applying Eqs. 17 and 18 with the measured data in Figures 13 and 14 are shown in Figure 16, the Nyquist plot for the hydrodynamic stability for a system of parallel channels operating on conditions specified in Figure 13 and Figure 14. The curve denoted "Single Channel Mode" in Figure 16 is the Nyquist plot for the in-phase mode of multi-channel oscillations, and the term denoted "Multi-Channel Mode" applies where the inter-channel phase relationship results in a complete cancellation of flow disturbance in the downcomer. Neither curve encircles the -1 point and hence the system is hydrodynamically stable in both modes.* The curve for the single channel mode crosses the real axis at a frequency of about 3 radians per second, corresponding to an experimentally observed peak in the natural circulation flow response to power modulation at this frequency, of about 10 radians per second, indicating that the multi-channel mode of oscillation is a higher frequency phenomenon than the single channel mode, at least for the present case. Both modes of oscillation can occur simultaneously in a parallel channel system.

Inasmuch as the multi-channel mode produces no net disturbance in the downcomer flow, it follows that a forced circulation system, satisfying the assumptions in this analysis could also be analyzed by the above procedure. Hence, measurements on a single channel, yielding the required impedances, could enable predictions of parallel channel instabilities in a system of such channels under forced circulation.

---

*This is in agreement with experimental observation on the single channel mode.

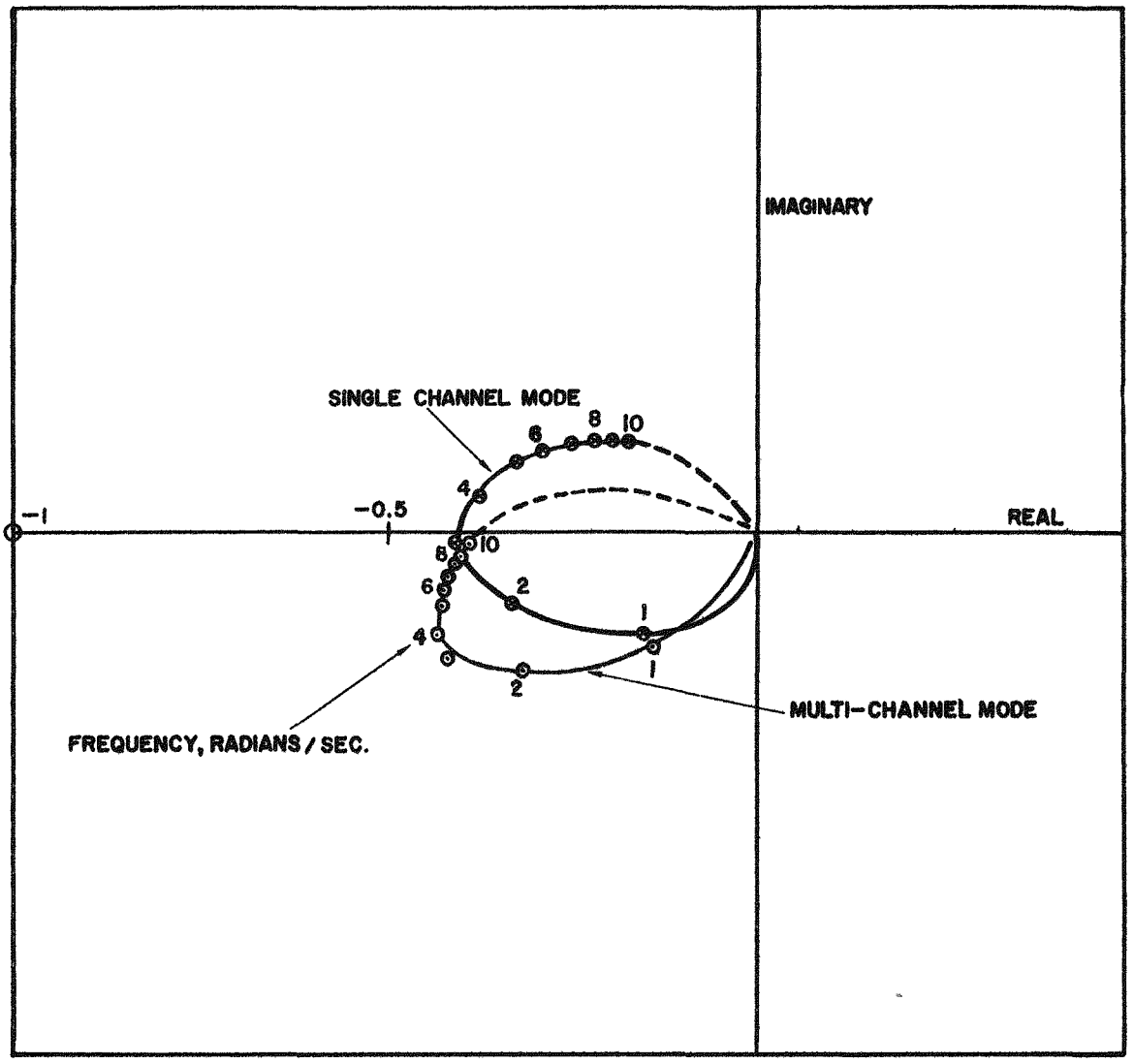


Figure 16. Nyquist Diagram for Hydrodynamic Stability of a System of Identical Parallel SPERT IA Channels, Each Operating at the Conditions of Figure 13. Impedance ratios used in this calculation were estimated from data in Reference 8, and are

$$\frac{Z_{SD} + Z_I}{Z_E} = - 0.18 - (0.20)\ j\omega$$

$$\frac{Z_I}{Z_E} = - 0.18 - (0.05)\ j\omega$$

## LIST OF REFERENCES

1. S. M. Zivi, "A Mechanism for Severe Pressure Transients in Heterogeneous Reactor Power Excursions", STL Quarterly Report 8977-6019-SU-000, 30 May 1962.

2. R. S. Margulies, "Temperature Rise in SPERT", a section of "Theory of Power Transients in the SPERT I Reactor" by W. A. Horning and H. C. Corben, Ramo Wooldridge Report ERL-109, 20 August 1957.

3. H. C. Corben, "Theory of Power Transients in the SPERT I Reactor", IDO-16434, 10 January 1958.

4. S. G. Forbes, "Calculation of Thermal Shutdown Effects in SPERT IA", Phillips Petroleum Co., SPERT Project Quarterly Progress Report, IDO-16512, 6 May 1959.

5. J. R. Dietrich, "Experimental Investigation of the Self-Limitation of Power During Reactivity Transients in a Subcooled Water Moderated Reactor, BORAX I Experiments, 1954", AECD-3668.

6. H. S. Carslaw and J. C. Jaeger, "Conduction of Heat in Solids", 2nd Ed., Oxford, p. 62, (1959).

7. S. M. Zivi, "Measurements and Interpretation of Transfer Functions and Hydrodynamic Instabilities in Boiling Loop Experiments", STL Quarterly Report 8977-6022-SU-000, 28 June 1962.

8. A. L. Morse, R. W. Wright, and S. M. Zivi, "Kinetic Studies of Heterogeneous Water Reactors - 1960 Annual Summary Report", RWD-RL-190.

9. Argonne National Laboratory, Reactor Development Program Progress Report, ANL-6509, January 1962.